Journal of Rock Mechanics and Geotechnical Engineering 6 (2014) 417–427

Contents lists available at ScienceDirect

Journal of Rock Mechanics and Geotechnical Engineering

journal homepage: www.rockgeotech.org

Full length article

Seismic earth pressures on flexible cantilever retaining walls with deformable inclusions

Ozgur L. Ertugrul [a,*], Aurelian C. Trandafir [b]

[a] Department of Civil Engineering, Mersin University, Ciftlikkoy 33343, Turkey
[b] Fugro GeoConsulting, Inc., Houston, TX 77081, USA

ARTICLE INFO

Article history:
Received 10 April 2014
Received in revised form
9 July 2014
Accepted 15 July 2014
Available online 26 August 2014

Keywords:
Cantilever retaining wall
Deformable geofoam panel
1-*g* shaking table tests
Dynamic earth pressure
Polystyrene
Flexibility ratio
Analytical approach

ABSTRACT

In this study, the results of 1-*g* shaking table tests performed on small-scale flexible cantilever wall models retaining composite backfill made of a deformable geofoam inclusion and granular cohesionless material were presented. Two different polystyrene materials were utilized as deformable inclusions. Lateral dynamic earth pressures and wall displacements at different elevations of the retaining wall model were monitored during the tests. The earth pressures and displacements of the retaining walls with deformable inclusions were compared with those of the models without geofoam inclusions. Comparisons indicated that geofoam panels of low stiffness installed against the retaining wall model affect displacement and dynamic lateral pressure profile along the wall height. Depending on the inclusion characteristics and the wall flexibility, up to 50% reduction in dynamic earth pressures was observed. The efficiency of load and displacement reduction decreased as the flexibility ratio of the wall model increased. On the other hand, dynamic load reduction efficiency of the deformable inclusion increased as the amplitude and frequency ratio of the seismic excitation increased. Relative flexibility of the deformable layer (the thickness and the elastic stiffness of the polystyrene material) played an important role in the amount of load reduction. Dynamic earth pressure coefficients were compared with those calculated with an analytical approach. Pressure coefficients calculated with this method were found to be in good agreement with the results of the tests performed on the wall model having low flexibility ratio. It was observed that deformable inclusions reduce residual wall stresses observed at the end of seismic excitation thus contributing to the post-earthquake stability of the retaining wall. The graphs presented within this paper regarding the dynamic earth pressure coefficients versus the wall flexibility and inclusion characteristics may serve for the seismic design of full-scale retaining walls with deformable polystyrene inclusions.

1. Introduction

Studies on the reduction of dynamic earth pressures of retaining walls have gained significant importance during this decade. Within these studies, utilization of geofoam inclusions appears as an innovative approach to reduce the earth pressures on retaining walls. Several studies focused on the potential load reduction efficiency of geofoam inclusions, indicating that the reduction performance of the geofoam inclusions depends on characteristics of the dynamic excitation, and mechanical characteristics of the backfill and deformable material.

Athanasopoulos et al. (2007), Bathurst et al. (2007), Zarnani and Bathurst (2009), and Ertugrul and Trandafir (2011) investigated the reduction of dynamic earth pressures of yielding rigid walls by compressible inclusions. Subsequently, Trandafir and Ertugrul (2011) discussed the influence of geofoam inclusions on reducing lateral dynamic earth pressure and displacements of a yielding gravity retaining wall subjected to a real earthquake excitation. Athanasopoulos-Zekkos et al. (2012) used deformable inclusions to reduce the seismic incremental earth pressures and displacements of yielding gravity type earth retaining walls.

In a recent study, Ertugrul and Trandafir (2013) discussed the results of 1-*g* static loading tests performed on cantilever retaining walls with EPS and XPS geofoam inclusions. In this study, only static load reduction efficiency of geofoam was investigated. Based on the static test results, a finite element model was analyzed and the outputs of the numerical model were validated using test data. Parametric analyses were performed to investigate the effect of

* Corresponding author. Tel.: +90 533 393 70 66.
E-mail addresses: ozgurertugrul@hotmail.com, ertugrul@mersin.edu.tr (O.L. Ertugrul).
Peer review under responsibility of Institute of Rock and Soil Mechanics, Chinese Academy of Sciences.
1674-7755
http://dx.doi.org/10.1016/j.jrmge.2014.07.004

different backfill and geofoam characteristics as well as structural performances of the cantilever walls. Formulas were proposed to estimate the static load reduction efficiency of geofoam inclusions placed against retaining walls with different characteristics. In the current investigation, dynamic response of cantilever earth retaining walls with deformable inclusions subjected to dynamic loads are discussed based on 1-*g* shaking table test results.

2. Methodology of the study

The present study focuses on the reduction of dynamic earth forces of yielding cantilever retaining walls caused by deformable geofoam inclusions. Deformable inclusion properties, flexibility of the retaining wall, granular backfill characteristics and the excitation parameters significantly increase the complexity of the mechanism of dynamic load reduction mechanism induced by the deformable panels of geofoam. Under such circumstances, physical testing with shaking table serves as a versatile tool to investigate this complex soil-geofoam-structure interaction. In the present study, the results of 1-*g* shaking table tests performed on small-scale flexible cantilever wall models using either the granular backfill or the deformable geofoam panel-granular backfill system are presented and discussed. Tests were conducted in a state-of-the-art laminar container to reduce the disturbance of the model response from wave reflections encountered in dynamic tests performed in the rigid containers. Influences of wall stiffness, geofoam type, inclusion thickness and seismic excitation characteristics (frequency and amplitude) on the dynamic earth pressures and wall displacements were investigated.

Results of the current study were also compared with those of analytical Steedman–Zeng methodology (Steedman and Zeng, 1990), which was validated using data obtained from physical tests performed on centrifuge facility.

3. Physical tests

The 1-*g* physical tests performed on small-scale geotechnical models, an inexpensive and efficient way to investigate the behavior of the prototype qualitatively. However, these tests have their own disadvantages, e.g. the requirements of the dimensional similitude theory may not be fully fulfilled in 1-*g* physical model tests. Some published papers (Hazarika et al., 2003; Bathurst et al., 2007) also discussed 1-*g* shaking table test results without mentioning prototype dimensions and the dimensional similitude relationships. In content, dynamic centrifuge tests are more successful in satisfying the similitude relationships between the prototype and the model (Wang et al., 2005; Wang, 2012). Nevertheless, dynamic 1-*g* tests can provide a source of reliable data for supporting numerical modeling and back analysis (Wood, 2004).

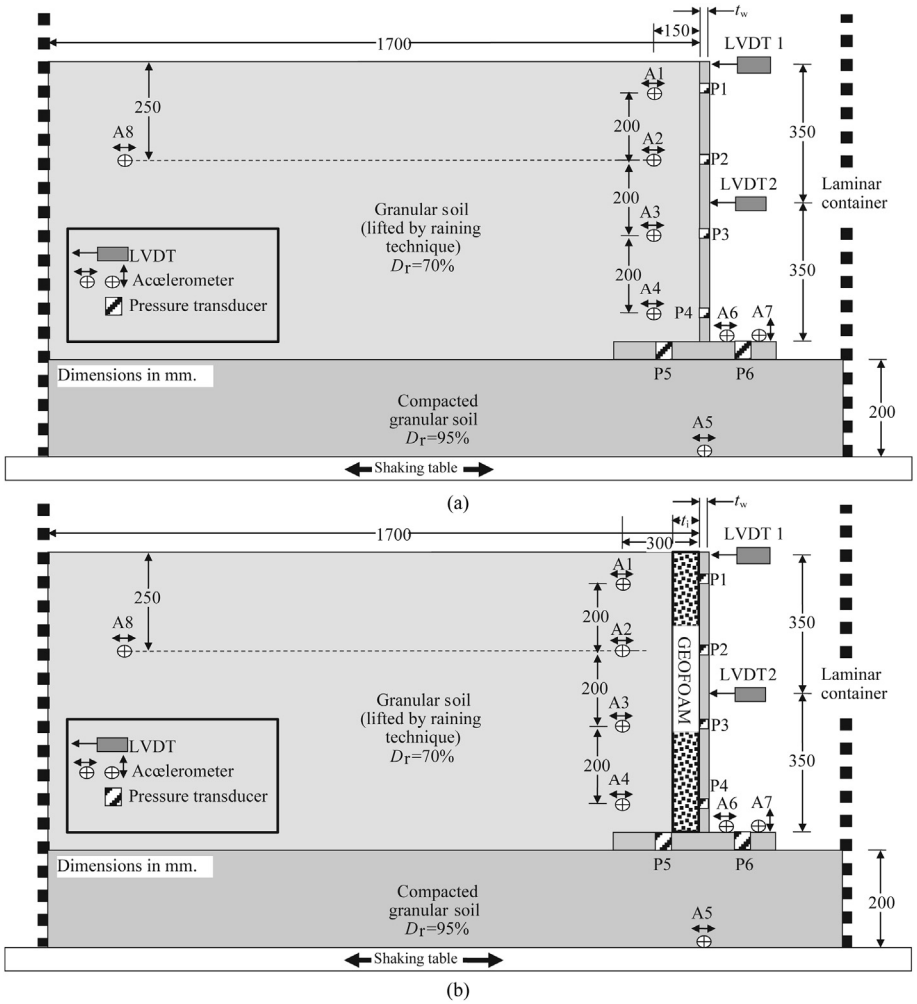

Fig. 1. Cross-sectional view of the model configurations. (a) Control test; (b) Wall with geofoam inclusion.

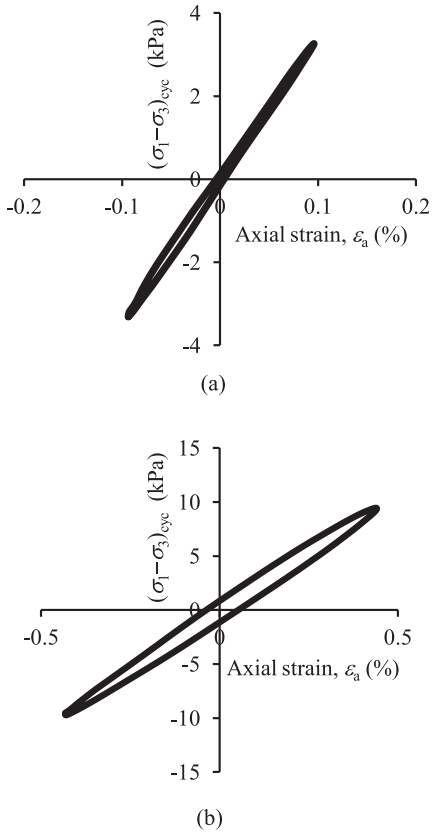

Fig. 2. Typical cyclic stress–strain loops for EPS15 (f = 3 Hz; N = 10 cycles). (a) $\Delta(\sigma_1 - \sigma_3)_{cyclic}$ = 3 kPa, (b) $\Delta(\sigma_1 - \sigma_3)_{cyclic}$ = 12 kPa.

Physical tests were conducted using a rectangular laminar sand container available in the Department of Civil Engineering at the Middle East Technical University. The uniaxial container with dimensions of 1.0 m × 1.5 m × 1.0 m (length × width × height) consists of laminar frames, low friction linear and ball bearings, guide walls to limit vertical dilatational movements of the frames and a thin membrane made of rubber to prevent material leakage when the laminar frames are moving.

Pressure and displacement transducers were mounted along the wall height to monitor pressures and displacements of the wall stem. Accelerometers were placed at different heights within the backfill and on the wall to monitor horizontal and vertical accelerations. A cross-sectional view of the test set-up and positions of the transducers are depicted in Fig. 1. The model walls are composed of steel with dimensions of 700 mm × 980 mm × (2-4-5-8) mm (height × length × thickness) rigidly welded to a steel base with dimensions of 980 mm × 500 mm × 8 mm (length × width × thickness). The connection of the wall stem to the wall foundation was achieved by welding. Signals from the transducers were recorded by a digital data acquisition hardware capable of 100 kHz sampling at each channel and signal conditioning elements for the required channels.

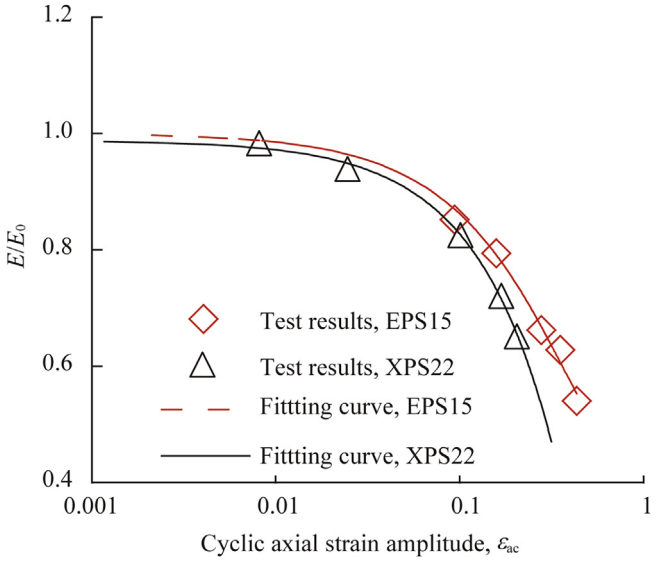

Fig. 3. Normalized Young's modulus (E/E_0) in relation to the cyclic axial strain amplitude ($(\sigma_1 - \sigma_3)_{static}$ = 15 kPa and $\Delta(\sigma_1 - \sigma_3)_{cyclic}$ = 3–14 kPa).

4. Material characteristics

The geotechnical properties of the dry cohesionless backfill material used in the tests was described by Ertugrul and Trandafir (2011). The granular material is classified as poorly graded sand (SP) which consists of highly angular grains. The maximum and minimum void ratios of the model sand were determined as 0.745 and 0.436, respectively, according to the procedure described by Head (1992). Specific gravity (G_s) was determined as 2.66 from the tests performed following ASTM D854-83 procedures. Consolidated-drained triaxial tests yielded an internal friction angle and dilatancy angle of 43.5° and 22.5°, respectively, for an effective confining stress range of 5–15 kPa.

The densities of EPS and XPS geofoam materials used as deformable panels in the physical tests were determined as 15 kg/m^3 and 22 kg/m^3, respectively. Low-density geofoam products were carefully selected for this study in order to provide a low stiffness buffer between the wall and the cohesionless backfill, thus allowing for soil lateral displacements induced by the compression of the deformable zone at very low confining stresses.

Static and cyclic triaxial tests were carried out on geofoam samples to determine the stress–strain relationship. Cylindrical specimens having a height to diameter ratio of 2 were extracted from EPS and XPS panels by computer-controlled laser cutters at ACH Foam Technologies LLC, Salt Lake City, Utah. The uniaxial compression tests on geofoam for EPS15 and XPS22 provided yield stresses of 39 kPa and 131 kPa, respectively, at a strain rate of 10^{-4} min^{-1}. The strain rate was consistent with the loading rate of the geofoam panels during the backfilling process of the 700-mm high retaining wall models in the physical tests.

According to the triaxial test results, EPS geofoam basically exhibits bi-linear stress–strain behavior with strain hardening occurring at 2% axial strain. Elastic modulus (E_i) representing the linear elastic portion was determined as 1500 kPa from monotonic

Table 1
A summary of the test parameters.

Wall type	Wall flexibility ratio, d_w	Inclusion material	Inclusion thickness ratio, t_i/H	Excitation frequency, f (Hz)	Acceleration amplitude, a_{max} (g)
I*	128	**E**: EPS15, **X**: XPS22 or **N**: no inclusion	**7**: 0.07 or **14**: 0.14	4–10	0.1–0.7
II	524				
III	1024				
IV	8197				

Note: *Bold letters are used to express test series in abbreviated form (e.g. **Type-II-E7** is the abbreviated form to indicate the wall model having d_w = 524 and EPS15 geofoam inclusion possessing t_i/H of 0.07).

loading tests. The measured elastic modulus of the EPS used in the current study is significantly lower than that estimated by the relationship suggested by Horvath (1995). One important cause of the low elastic modulus reported in the current study is the low strain rate (10^{-4} min^{-1}) that has been adopted in the compression tests performed. Most of the relationships in the literature between the elastic modulus and the density of the geofoam were based on the monotonic test results performed with a customary strain rate of 10^{-1} min^{-1} (Koerner, 2005). Duskov (1997) reported that loading rate significantly affects the stiffness of the EPS geofoam.

XPS geofoam exhibits a well-defined yield point in association with strain softening after yielding. Elastic modulus representing the linear elastic portion was determined as 5580 kPa. The triaxial test results also revealed that an increase in the confining stresses causes a decrease in the elastic modulus and yields deviatoric stress of geofoam.

Stress-controlled cyclic triaxial tests were performed on EPS15 and XPS22 samples to determine the dynamic modulus (E_{dyn}) and the maximum axial strain (ε_{max}) under dynamic loads. During the tests, cyclic component of the axial stress remained below the static confining stresses initially applied to the samples. Fig. 2 shows the viscoelastic stress–strain response of EPS geofoam at different cyclic deviatoric stress levels. Based on the data obtained from cyclic triaxial tests, the Young's moduli (E) of the geofoam at different axial strains were normalized with initial modulus (E_0) to develop E/E_0 degradation curves for EPS and XPS geofoams in relation to the cyclic axial strain amplitude, as shown in Fig. 3.

In the tests, cyclic axial strain amplitudes (ε_{ac}) up to about 0.50% were observed. According to the results proposed by Trandafir and Erickson (2012), geofoam exhibits visco-elasto-plastic behavior after exceeding threshold of axial strain amplitude of 0.54%. Hence, the dynamic properties of the EPS and XPS geofoams reported in this study are representative for the viscoelastic behavior of these materials. The initial Young's moduli of EPS15 and XPS22 corresponding to a cyclic strain amplitude $\varepsilon_{ac} = 0.01\%$ were estimated as 4745 kPa and 8907 kPa, respectively, using the following equation proposed by Trandafir and Erickson (2012):

$$E_0 = 59.93\rho^2 - 1622.8\rho + 15602 \quad (1)$$

where E_0 and ρ are expressed in kPa and kg/m^3, respectively. The initial Young's moduli estimated by Eq. (1) were found to be in agreement with the results of the laboratory tests performed in this study. Trandafir and Erickson (2012) indicated that results from cyclic uniaxial compression tests performed on EPS geofoam reveal insignificant variation in the Young's modulus for cyclic axial strain amplitudes of up to 5×10^{-4}. Thus, the measured Young's modulus values at cyclic axial strain amplitudes not greater than 5×10^{-4} in cyclic uniaxial compression tests may be appropriate to describe the small strain elastic behavior of geofoam.

5. Test procedure

The instrumented retaining wall models were placed on the 20-cm thick compacted layer of sand. During the backfilling process, the wall model was kept fixed against horizontal movements by means of lateral supports. Backfill was constituted of 10-cm lifts by dry pluviation, a commonly used method to reconstitute granular materials representative of some initial state (Okamoto and Fityus, 2006). To make use of dry pluviation technique, a steel shutter and diffuser screen having the same dimensions with the laminar container were manufactured. Based on the test results presented by Okamoto and Fityus (2006), hole spacing of the shutter and diffuser screen were selected as 60 mm and 2.36 mm, respectively, in order to obtain relative densities between 70% and 75% by raining procedure. At the end of the backfilling process, the data acquisition equipment was used to monitor wall pressures on the non-yielding wall (lateral restraints were presented). The data

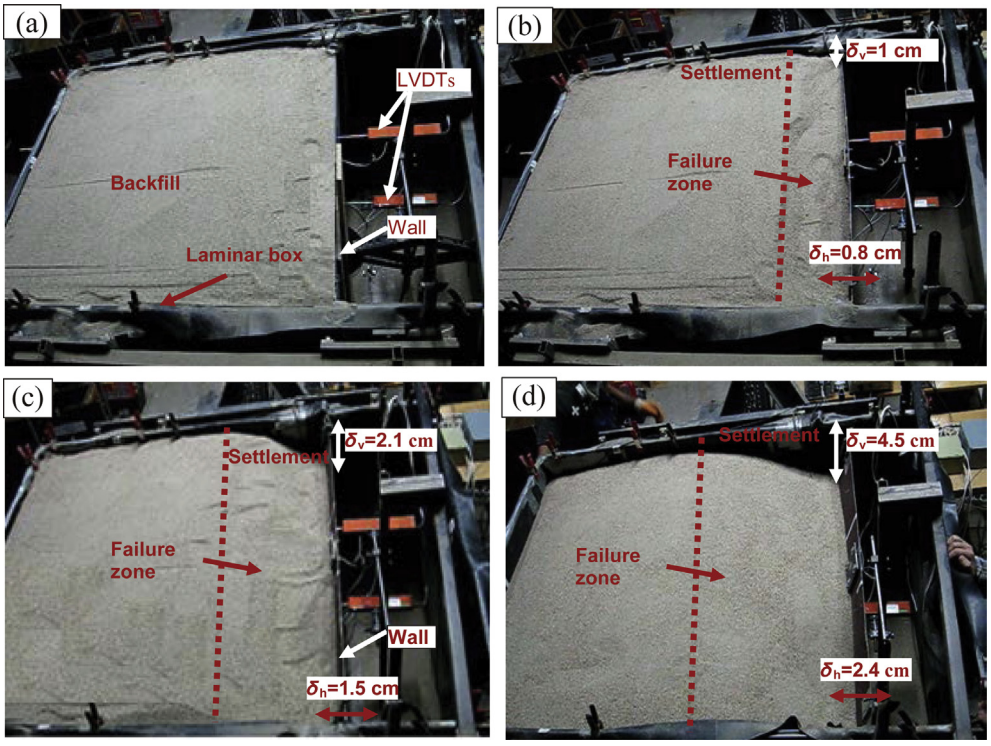

Fig. 4. Retaining wall model ($d_w = 524$) without deformable inclusion; (a) Before the dynamic phase; (b) After 0.1 g-4 Hz excitation; (c) After 0.4 g-8 Hz excitation; (d) After 0.7 g-10 Hz excitation.

acquisition continued during the removal of the restraints accomplished by the slow unloading of the mechanical jack located between the wall model and the sides of the container. Lateral earth pressures and wall movements were monitored until no further wall movements and pressure redistribution occurred. The tests involving compressible geofoam inclusions were carried out following the same procedure. However, EPS and XPS geofoam panels were installed between the wall model and the backfill prior to the pluviation. Direct shear tests were performed to determine the interface friction between the geofoam and the granular material. The friction coefficient of the contact plane between the geofoam and the granular backfill was found as 0.13 since the surfaces of the geofoam panels used in the current study were covered with plastic tape to reduce the friction between the soil and the geofoam. With decreasing frictional force at the geofoam–backfill interface, the loading axis of the earth thrust becomes closer to horizontal. In the shaking table tests, harmonic displacements matching the following target sinusoidal acceleration-time history were applied to the base of the laminar container by means of dynamic actuator:

$$a_h(t) = \begin{cases} \frac{a_{max}}{4} ft \sin(2\pi ft) & \left(t < \frac{4}{f}\right) \\ a_{max} \sin(2\pi ft) & \left(\frac{4}{f} \le t < 5\right) \\ \frac{a_{max}}{4}\left[\left(5+\frac{4}{f}\right) - t\right] f \sin(2\pi ft) & \left(5 \le t \le 5+\frac{4}{f}\right) \end{cases} \quad (2)$$

where t is the time, f is the frequency of the excitation, and a_{max} is the acceleration amplitude. Although the application of random earthquake excitations in physical modeling studies is considered more realistic, Bathurst and Hatami (1998) and Matsuo et al. (1998) reported that simple harmonic base excitations can cause more aggressive impact on the physical model when compared with the effect of a real earthquake excitation with similar predominant frequency and amplitude. Additionally, application of harmonic base motion allows the physical models to be excited in the same controlled way by enabling more accurate comparisons to be made regarding the effect of different input parameters investigated in this study. A summary of the test parameters is listed in Table 1.

Retaining wall models having different stem thicknesses were used to investigate the influence of relative flexibility of the retaining structure on the seismically induced earth pressures and the performance of deformable geofoam inclusions. Plane strain relative flexibility ratio (d_w) of a retaining wall is considered as the primary parameter affecting the response of the cantilever wall-backfill system (Veletsos and Younan, 1997) and is expressed in a dimensionless form as

$$d_w = 12\left(1-\nu_w^2\right)\frac{G}{E_w}\left(\frac{H}{t_w}\right)^3 \quad (3)$$

where G is the shear modulus of the backfill, H is the wall height, E_w is the Young's modulus of the wall, t_w is the wall thickness, and ν_w denotes the Poisson's ratio of the material. Relative flexibility ratios for four model walls were determined as 128, 524, 1024 and 8197 when calculated using Eq. (3).

6. Discussion of the test results

Residual wall displacements and surface settlements of the backfill at the end of different seismic excitation phases are

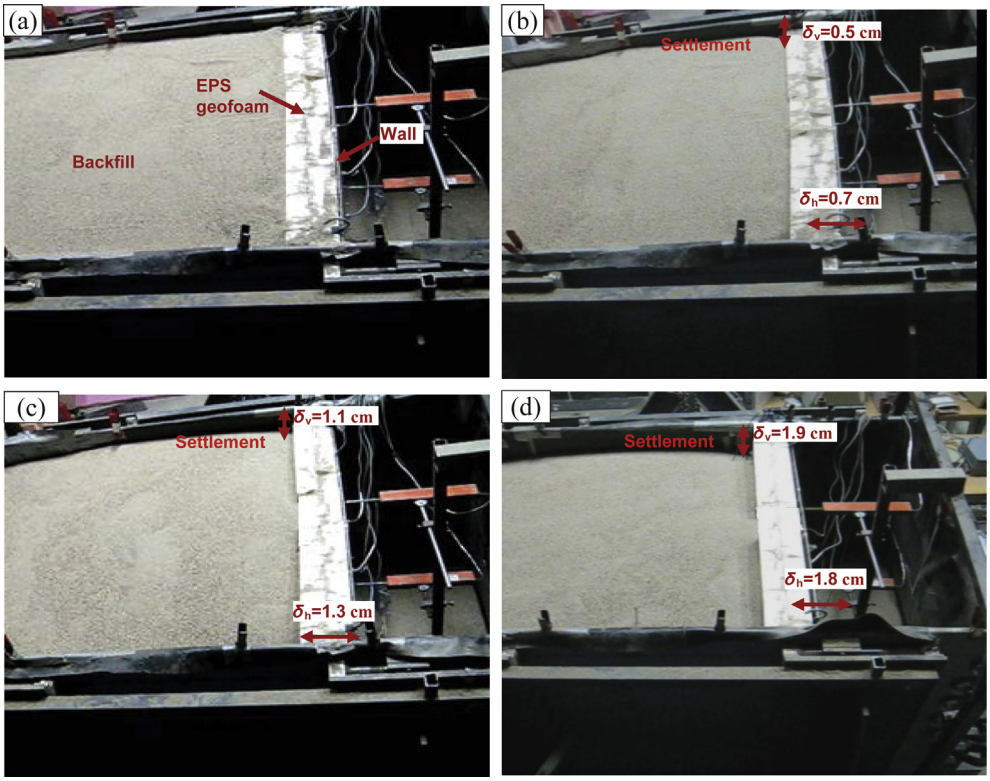

Fig. 5. Retaining wall model (d_w = 524) with EPS15 deformable inclusion having t_i/H = 0.14. (a) Before the dynamic phase; (b) After 0.1 g-4 Hz excitation; (c) After 0.4 g-8 Hz excitation; (d) After 0.7 g-10 Hz excitation.

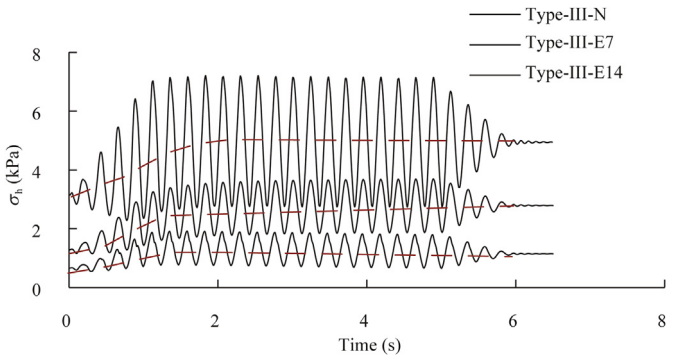

Fig. 6. Evolution of the dynamic wall pressures monitored at the wall base ($a_{max} = 0.3$ g, $f = 4$ Hz).

depicted in Figs. 4 and 5. It is indicated that horizontal displacements and backfill settlements increase as the excitations with higher amplitude and frequency were applied to the model. EPS15 geofoam panel having a relative thickness (i.e. ratio of panel thickness, t_i, to wall height, H) $t_i/H = 0.14$ caused a significant increase in the backfill settlement as a result of the compressive deformations of the geofoam panel.

In the test series without geofoam panels, the surface settlements at the end of the test were significantly lower when compared with those of the geofoam tests. It was observed that the flexural wall deformations and the reduction in the backfill volume due to dynamic densification are the primary factors causing settlement for the tests without geofoam. However, installation of a compressible element between the wall stem and the granular backfill introduces another factor, i.e. compressible deformations of the geofoam layer, which causes additional surface settlements. Horvath (2010) defined a dimensionless parameter (λ) called the normalized compressible inclusion stiffness:

$$\lambda = \frac{EH}{t_i P_{atm}} \tag{4}$$

where P_{atm} is the atmospheric pressure, in the same units as E, used to make λ dimensionless. Parameter "λ" is dependent on H/t_i as can be observed from the given formula. In the current investigation, the authors defined t_i/H as the relative thickness and used this parameter in the discussions. During the tests, it was observed that the settlement in the vicinity of the wall increases as t_i/H increases.

In the dynamic tests, the granular backfill subjected to dynamic base excitation was densified, causing higher lateral stresses in the backfill compared with the initial condition. As the lateral loads of the geofoam buffer increases permanently due to soil densification, compressive deformations of the geofoam panels continuously increase, causing progressive vertical backfill settlements in the vicinity of the wall. While the compressive deformations in the geofoam panels increase, higher volume of granular backfill moves in the horizontal direction towards the wall. This causes additional vertical backfill settlements concentrated in the vicinity of the wall. As the relative thickness ratio (t_i/H) of the geofoam inclusion increases, the additional vertical settlements are induced by compressive deformations of the geofoam.

6.1. Dynamic wall pressures and lateral displacements

In Fig. 6, the total dynamic earth pressures at the depth $z = H$ (i.e. wall base) were compared for Type-III wall models ($d_w = 524$) subjected to a base excitation characterized by $a_{max} = 0.3$ g and $f = 4$ Hz. Initial static stresses as well as the dynamic incremental stresses for the walls with EPS15 geofoam inclusions were found to be lower than those of the model without deformable inclusion. The increments of dynamic stresses for Type-III-E7 and Type-III-E14 models (EPS15 inclusion with $t_i/H = 0.07$ and $t_i/H = 0.14$, respectively) were significantly lower compared with the control case of the wall without geofoam inclusion (Type-III-N).

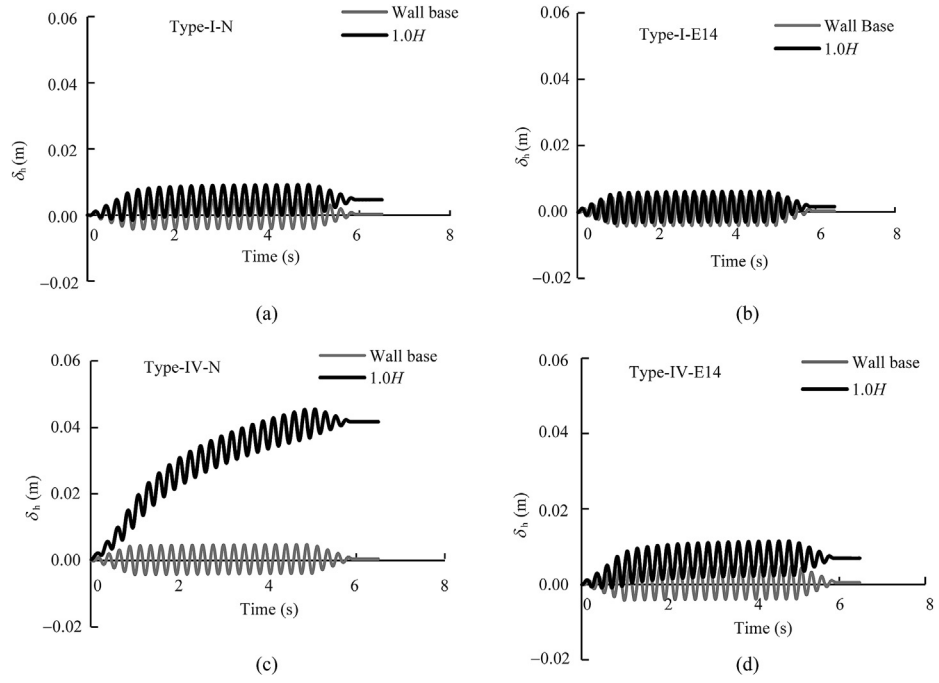

Fig. 7. Evolutions of wall displacements for (a) Type-I-N; (b) Type-I-E14 ($d_w = 128$); (c) Type-IV-N; (d) Type-IV-E14 ($d_w = 128$).

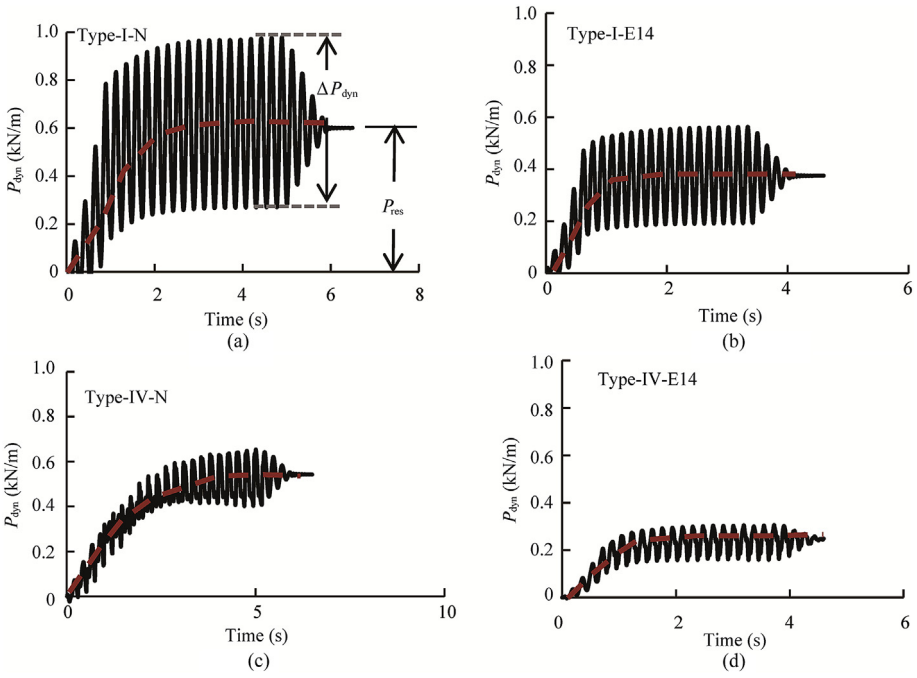

Fig. 8. Evolution of the total dynamic thrust for (a) Type-I-N; (b) Type-I-E14 ($d_w = 128$); (c) Type-IV-N; (d) Type-IV-E14 ($d_w = 8197$).

The evolutions of lateral displacements at the wall top during dynamic phase ($a_{max} = 0.3\,g$ and $f = 4$ Hz) for the most rigid (Type-I, $d_w = 128$) and the most flexible models (Type-IV, $d_w = 8197$) are compared in Fig. 7. The horizontal displacements monitored at the top (indicated with bold lines) of the model Type-I (Fig. 7a) are significantly lower than those observed for the more flexible model wall Type-IV (Fig. 7c). Residual wall displacements (δ_{res}) increase as wall flexibility ratio increases. EPS15 geofoam inclusions with $t_i/H = 0.14$ significantly reduce the dynamic incremental and residual wall displacements (Fig. 7b and d).

Based on the comparisons of the lateral dynamic pressure and wall displacements with different flexibility ratios, it can be noted that the earth pressure against the rigid walls was reduced by the within-backfill deformations induced by the lateral compression of the low stiffness inclusion. The widespread backfill settlements were considered to be an indicator of the compressive deformations of the geofoam panel. This positive effect of the deformable geofoam panels also reduces the flexural displacements of the wall stem in association with the load reduction behavior. Pressures and displacements of the walls with XPS geofoam panel were not presented in Figs. 6 and 7. However, it can be said that the XPS deformable panels have slightly low efficiency compared with the performance of the EPS geofoam panels.

The evolution of the total dynamic lateral force of model walls Type-I and Type-IV is depicted in Fig. 8. Wall flexibility has an effect on the residual earth force (P_{res}) as well as on the dynamic component (ΔP_{dyn}) of the total thrust (Fig. 8a and c). EPS15 geofoam with $t_i/H = 0.14$ provides significant reduction in P_{res} and ΔP_{dyn} for both of the models (Fig. 8b and d).

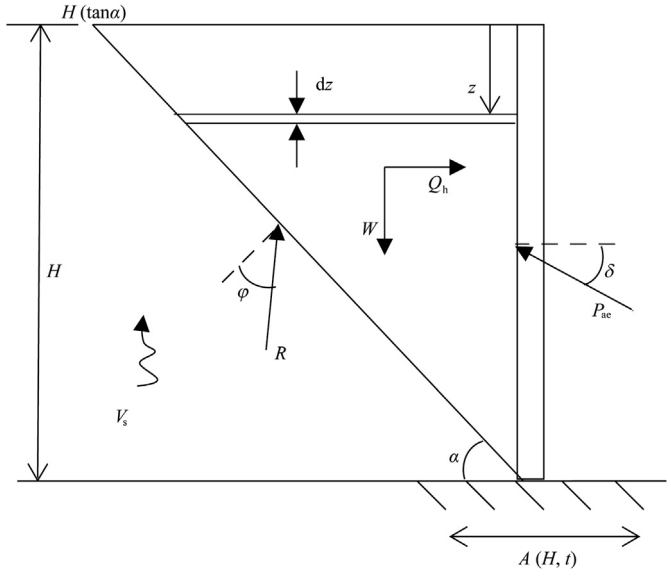

Fig. 9. The parameters used in the calculation of the dynamic earth forces according to Steedman–Zeng method (1990).

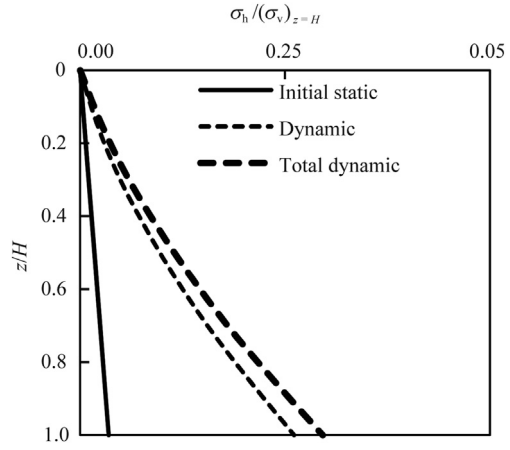

Fig. 10. Normalized earth pressure profiles calculated with Steedman–Zeng method ($a_{max} = 0.3\,g$ and $f = 5$ Hz).

6.2. Comparisons of the test data with the results obtained by Steedman–Zeng method

One of the important studies addressing the evaluation of dynamic lateral earth pressures of fixed base cantilever retaining walls was presented by Steedman and Zeng (1990). In this study, the authors proposed an analytical methodology which took into account the shear wave velocity distribution within the backfill, thus allowing for a phase difference and variable acceleration profile in a prototype. Centrifuge test data exhibited a good agreement with the results obtained by the analytical methodology well known as Steedman–Zeng (S–Z) method.

The parameters used in the calculation of seismic forces with the analytical approach suggested by Steedman and Zeng (1990) are presented in Fig. 9. The harmonic base excitation is written as

$$A(z,t) = k_h g \sin\left[\omega\left(t - \frac{H-z}{V_s}\right)\right] \tag{5}$$

where k_h is the horizontal acceleration amplitude, V_s is the shear wave velocity of the backfill, ω is the angular frequency of the base shaking, and z is the elevation measured from the wall top. For a typical fixed base cantilever wall, the horizontal inertia force Q_h acting on a horizontal element (thickness of dz) of the failure wedge within the backfill is given by

$$Q_h = \int_0^H \rho\left(\frac{H-z}{\tan\alpha}\right) A(z,t)\mathrm{d}z \tag{6}$$

where ρ is the density of the backfill, and α is the inclination angle of wedge with the horizontal direction. The total dynamic thrust is calculated with the following equation considering the equilibrium of the forces acting on the wedge shown in Fig. 9:

$$P_{ae} = \frac{Q_h \cos(\alpha-\varphi) + W\sin(\alpha-\varphi)}{\cos(\delta-\alpha+\varphi)} \tag{7}$$

where W is the weight of the soil wedge, φ is the angle of soil shear resistance, and δ is the angle of wall friction. The total lateral earth pressure coefficient is thus obtained as

$$K_{ae} = \frac{2P_{ae}}{\gamma H^2} \tag{8}$$

The distribution of the total lateral pressure $p_{ae}(z)$ is expressed as

$$\left.\begin{aligned} p_{ae}(z) &= \frac{\partial P_{ae}(z)}{\partial z} = \frac{\cos(\alpha-\varphi)k_h\gamma z}{\cos(\delta-\alpha+\varphi)\tan\alpha}\sin\left[\omega\left(t-\frac{z}{V_s}\right)\right] \\ &\quad + \frac{\gamma z}{\tan\alpha}\frac{\sin(\alpha-\varphi)}{\cos(\delta-\alpha+\varphi)} \\ p_{ae}(z) &= p_{ad}(z) + p_{as}(z) \end{aligned}\right\} \tag{9}$$

where $p_{ad}(z)$ and $p_{as}(z)$ are the dynamic and static components of the total lateral pressure, respectively. The loading point of the dynamic thrust can be expressed by

$$H_d = \frac{M_d(z=H)}{P_{ad}\cos\delta} = \int_0^H \frac{p_{ad}(z)\cos\delta(H-z)\mathrm{d}z}{P_{ad}\cos\delta} \tag{10}$$

where $M_d\,(z=H)$ is the total bending moment at the fixed base, and P_{ad} is the dynamic component of the total thrust. Earth pressure profiles calculated with the analytical method and those obtained from physical tests are presented in Figs. 10 and 11, respectively. The

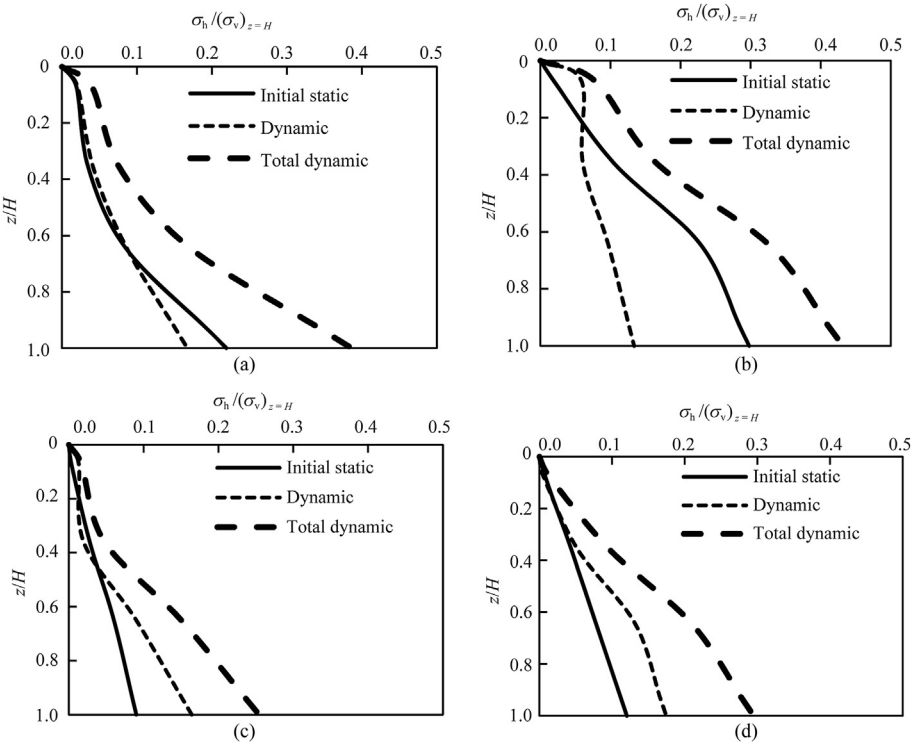

Fig. 11. Normalized pressure profiles ($a_{max} = 0.3\,g$ and $f = 5$ Hz). (a) $d_w = 1024$, without geofoam panel; (b) $d_w = 524$, without geofoam panel; (c) $d_w = 1024$, EPS15 with $t_i/H = 0.14$; (d) $d_w = 524$, EPS15 with $t_i/H = 0.14$.

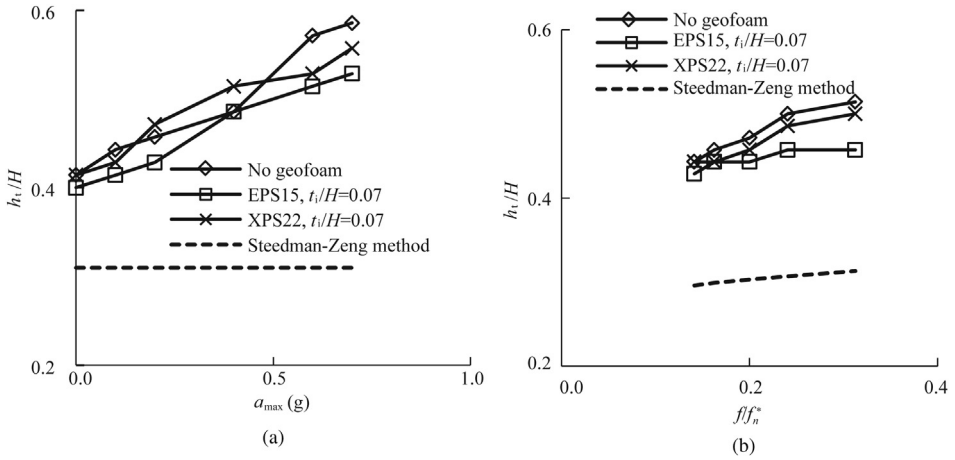

Fig. 12. Location of maximum thrust in relation to (a) Acceleration amplitude, a_{max} (for $f/f_n^* = 0.32$); (b) Frequency ratio, f/f_n^* (for $a_{max} = 0.7\ g$).

total earth pressures observed along the wall height are in good agreement with those calculated with the analytical procedure. However, the initial static and dynamic components were found to be significantly different from those estimated by the analytical method. According to the test results presented in Fig. 11, it can be inferred that the lateral arching behavior of the granular backfill leads to the formation of nonlinear pressure profiles along the wall. Regarding the static and dynamic components of the total earth force, the discrepancy between the test data and the results of the analytical study could be explained with the arching effects presented in the physical model. Pressures estimated with the analytical methodology were found to be more representative for the Type-I with low flexibility ratio, $d_w = 128$ (comparison of Figs. 10 and 11b).

The ratio of the dominant excitation frequency to the fundamental frequency of the wall–backfill system plays a major role in the magnitude of seismic pressures and wall displacements. In order to make comparisons of the seismic forces in relation to the frequency ratio achieved in the tests, the first fundamental frequency (f_n) of an equivalent one-dimensional linear elastic soil column can be estimated by a known height (H), shear modulus (G) and backfill density (ρ) as follows:

$$f_n = \frac{\sqrt{G/\rho}}{4H} \tag{11}$$

The modified natural frequency (f_n^*) of a backfill-retaining wall system was approximated as 32 Hz using the following shape factor suggested by Wu (1994):

$$\left.\begin{aligned} f_n^* &= Sf_n \\ S &= \sqrt{1+\left(\frac{1}{2-\nu}\right)}\left(\frac{H}{B}\right)^2 \end{aligned}\right\} \tag{12}$$

where B is the width of the two-dimensional model. Considering the backfill height and the fundamental frequency of the backfill-retaining wall system for the tests carried out within this study, phase differences within the backfill could not be observed. However, amplification of the base motion within the backfill could be observed for the range of investigated excitation characteristics. Since this study was performed on small-scale wall models in 1-g environment, backfill phasing effects were out of the scope of the investigation.

Loading points (h_t/H) of the total dynamic thrust for different excitation characteristics are presented in Fig. 12. According to the test data, the loading point of total thrust is estimated between 0.4H and 0.6H from the wall base. However, the loading point calculated with the analytical method is lower. This discrepancy originates from the shape of the total dynamic pressure profiles of the physical tests and those calculated with analytical method.

6.3. Dynamic earth pressure coefficients (K_{ae})

In Figs. 13–15, the lateral earth pressure coefficients (K_{ae}) are depicted for wall models with different flexibility ratios and deformable inclusion characteristics. According to Fig. 13, increase of a_{max} causes a nonlinear increase in K_{ae} values. A good agreement can be noted between the coefficients calculated with the analytical method and the test data corresponding to the wall without deformable buffer. The earth pressure coefficients shown in Fig. 13 were calculated from test data obtained from the rigid wall model Type-I ($d_w = 128$). On the other hand, wall flexibility has a prominent role in the dynamic earth pressures as demonstrated in Fig. 14. According to the test results, the total lateral dynamic forces decrease as the flexibility ratio of the wall increases. Deformable geofoam inclusions reducing earth pressure coefficients depends on the inclusion characteristics and flexural attributes of the wall. As observed in Fig. 14, the inclusion with the smallest stiffness ratio (E_i/t_i) provides the highest reduction. For the wall model Type-I ($d_w = 128$), EPS15 inclusion having $t_i/H = 0.14$ provides

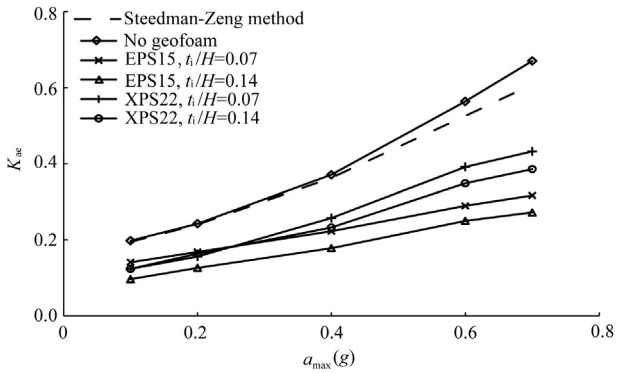

Fig. 13. Variation of dynamic earth pressure coefficient (K_{ae}) with a_{max} ($f/f_n^* = 0.15$) for the Type-I model ($d_w = 128$).

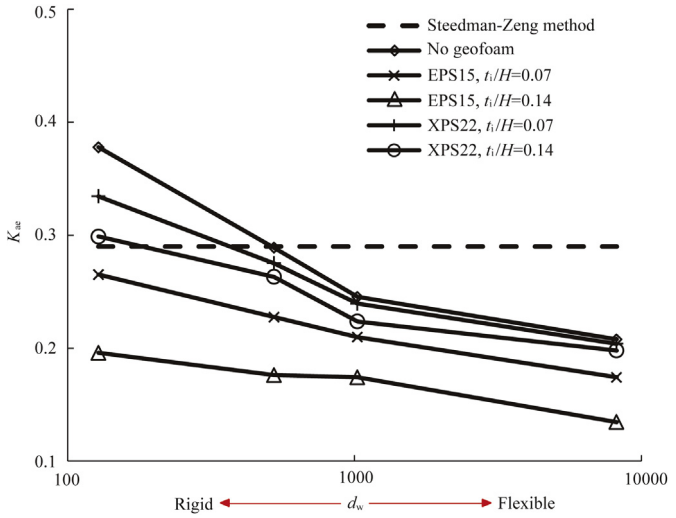

Fig. 14. Variation of dynamic earth pressure coefficient (K_{ae}) with d_w (base motion $f/f_n^* = 0.13$, $a_{max} = 0.3\ g$).

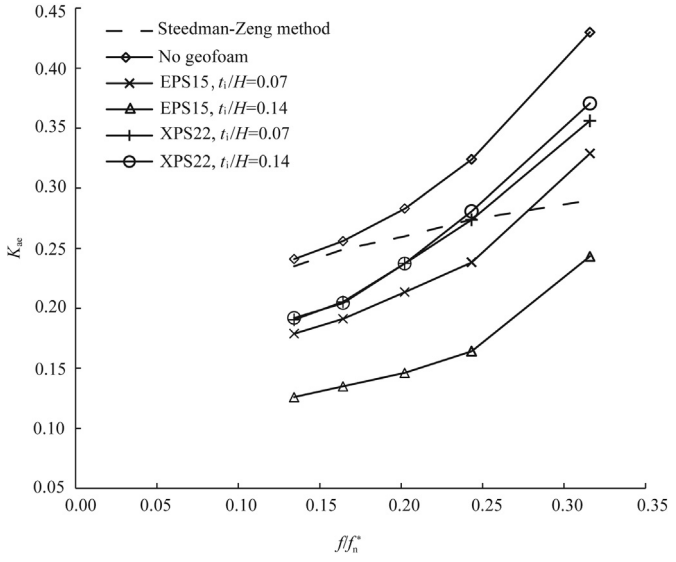

Fig. 15. Variation of dynamic earth pressure coefficient (K_{ae}) for wall Type-III with f/f_n^* ($a_{max} = 0.3\ g$, $d_w = 1024$).

approximately 50% decrease in K_{ae}. The same geofoam inclusion provides only 33% decrease in dynamic earth pressure coefficient for the model Type-IV ($d_w = 8197$). The influence of frequency ratio (f/f_n^*) on K_{ae} values for Type-III wall ($d_w = 1024$) is shown in Fig. 15. It can be observed that K_{ae} values significantly increase as (f/f_n^*) increases.

7. Conclusions

In this study, results of small-scale physical tests on flexible cantilever earth walls with deformable geofoam inclusions were presented. Wall models having different flexibility ratios were subjected to harmonic base excitations. Deformable inclusions possessing different stiffness and thickness characteristics were installed between the model walls and the cohesionless granular backfill to serve as the deformable layer. Test results indicated that the wall flexibility has a significant influence on the dynamic earth pressures. The dynamic earth forces and displacements of the walls with deformable panels were compared with those of the models without geofoam inclusions. Comparisons indicate that geofoam panels of low stiffness installed against the model retaining walls affect displacement and lateral pressure profile along the wall height. The efficiency of dynamic load and displacement reduction decreases as the flexibility ratio of the model wall increases. On the other hand, load reduction efficiency of the geofoam increases as the amplitude and frequency ratio of the seismic excitation increases. Relative flexibility of the deformable layer (the thickness and the elastic stiffness of the polystyrene material) plays an important role in reducing seismic earth forces. Depending on the inclusion characteristics and the wall flexibility, up to 50% reduction in dynamic lateral earth pressures may occur. According to the test results, the model retaining walls without geofoam inclusions experienced high residual stresses when subjected to the earthquake effect due to densification of the granular material. Deformable inclusions reduced residual wall stresses observed at the end of seismic excitation, thus contributing to the post-earthquake stability of the retaining wall. Loading point of the maximum dynamic thrust varies between $0.4H$ and $0.6H$, depending on the inclusion type, flexibility ratio of the wall and the characteristics of the harmonic motion applied to the base of the models. Dynamic earth pressure coefficients were compared with those calculated by the proposed analytical approach. Pressure coefficients calculated with this method were found to be in a good agreement with the testing results of the model walls with low flexibility ratio.

The presented graphs concerning the earth pressure coefficients versus the wall flexibility and inclusion characteristics may serve for the seismic design of full-scale retaining walls with deformable polystyrene inclusions.

Conflict of interest

We wish to confirm that there are no known conflicts of interest associated with this publication and there has been no significant financial support for this work that could have influenced its outcome.

References

Athanasopoulos-Zekkos A, Lamote K, Athanasopoulos GA. Use of EPS geofoam compressible inclusions for reducing the earthquake effects on yielding earth retaining structures. Soil Dynamics and Earthquake Engineering 2012;41:59–71.

Athanasopoulos GA, Nikolopoulou CP, Xenaki VC. Seismic Isolation of earth-retaining structures by EPS geofoam compressible inclusions—dynamic FE analyses. In: Proceedings of the 4th International Conference on Earthquake Geotechnical Engineering; 2007. Thessaloniki, Greece, Paper No. 1676.

Bathurst RJ, Hatami K. Seismic response analysis of a geosynthetic reinforced soil retaining wall. Geosynthetics International 1998;5(1/2):127–66.

Bathurst RJ, Zarnani S, Gaskin A. Shaking table testing of geofoam seismic buffers. Soil Dynamics and Earthquake Engineering 2007;27(4):324–32.

Duskov M. Materials research on EPS-20 and EPS-15 under representative conditions in pavement structures. Geotextiles and Geomembranes 1997;15(1–3):147–81.

Ertugrul OL, Trandafir AC. Lateral earth pressures on flexible cantilever retaining walls with deformable geofoam inclusions. Engineering Geology 2013;158:23–33.

Ertugrul OL, Trandafir AC. Reduction of lateral earth forces acting on rigid non-yielding retaining walls by EPS geofoam inclusions. Journal of Materials in Civil Engineering 2011;23(12):1711–8.

Hazarika H, Okuzono S, Matsuo Y. Seismic stability enhancement of rigid non-yielding retaining walls. In: Proceedings of the 13th International Offshore and Polar Engineering Conference, vol. 2. Cupertino, USA: International Society of Offshore and Polar Engineers (ISOPE); 2003. p. 697–702.

Head KH. Manual of soil laboratory testing. Soil classification and compaction tests. 2nd ed, vol. 1. London: Pentech Press; 1992.

Horvath JS. Geofoam geosynthetic. New York: P.C. Scarsdale; 1995.

Horvath JS. Lateral pressure reduction on earth-retaining structures using geofoams: correcting some misunderstandings. In: ASCE ER2010: Earth Retention Conference 3, Bellevue, USA; 2010.

Koerner RM. Designing with geosynthetics. 5th ed. Upper Saddle River, USA: Prentice Hall; 2005.
Matsuo O, Tsutsumi T, Yokoyama K, Saito Y. Shaking table tests and analysis of geosynthetic-reinforced soil retaining walls. Geosynthetics International 1998;5(1/2):97–126.
Okamoto M, Fityus SG. An evaluation of the dry pluviation preperation technique applied to silica sand samples. In: Geomechanics and Geotechnics of Particulate Media. London: Taylor and Francis Group; 2006. p. 33–9.
Steedman RS, Zeng X. The influence of phase on the calculation of pseudo-static earth pressure on a retaining wall. Geotechnique 1990;40(1):103–12.
Trandafir AC, Erickson BA. Stiffness degradation and yielding of EPS geofoam under cyclic loading. Journal of Materials in Civil Engineering 2012;24(1): 119–24.
Trandafir AC, Ertugrul OL. Earthquake response of a gravity retaining wall with geofoam inclusion. In: Geo-frontiers 2011: Advances in Geotechnical Engineering. Reston, USA: American Society of Civil Engineers; 2011.
Veletsos AS, Younan AH. Dynamic response of cantilever retaining walls. Journal of Geotechnical and Geoenvironmental Engineering 1997;123(2):161–72.
Wang MW, Iai S, Tobita T. Numerical modelling for dynamic centrifuge model test of the seismic behaviors of pile-supported structure. Chinese Journal of Geotechnical Engineering 2005;27(7):738–41 (in Chinese).
Wang MW. Dynamic centrifuge tests and numerical modelling for geotechnical earthquake engineering in liquefiable soils. Beijing: Science Press; 2012 (in Chinese).
Wood DM. Geotechnical modeling. 1st ed. New York: Spon Press; 2004.
Wu G. Dynamic soil structure interaction: pile foundations and retaining structures. PhD Thesis. Vancouver: The University of British Columbia; 1994.
Zarnani S, Bathurst RJ. Numerical parametric study of expanded polystyrene (EPS) geofoam seismic buffers. Canadian Geotechnical Journal 2009;46(3):318–38.

Dr. Ozgur L. Ertugrul is an assistant professor and graduate student supervisor in Department of Civil Engineering, University of Mersin. He obtained his M.S. and Ph.D. in Middle East Technical University. He earned Graduate Studies Performance Award in 2005 from Institute of Natural and Applied Sciences, Middle East Technical University. He made research on the dynamic characterization of geofoam in Department of Geology and Geophysics, University of Utah in 2009. His studies mainly concentrate on the seismic response of retaining walls, reduction of earth stresses with compressible inclusions, sesmic design of tunnels and underground structures. He has expertise on physical and numerical modeling of geotechnical problems. He has been involved in research projects funded by Turkish State Planning Organization, Middle East Technical University and Mersin University. He served as a consultant for ground improvement and deep excavations projects to the Turkish Government. He has published several papers on the seismic response of retaining walls and reduction of lateral earth stresses with deformable geofoam inclusions. He is a member of Turkish Society of Civil Engineers, Turkish National Committee of Soil Mechanics and Foundation Engineering, International Society for Soil Mechanics and Geotechnica Engineering. He makes paper reviews for journals such as Journal of Geotechnical and Geological Engineering, Lanslides and ASCE Journal of Materials in Civil Engineering.